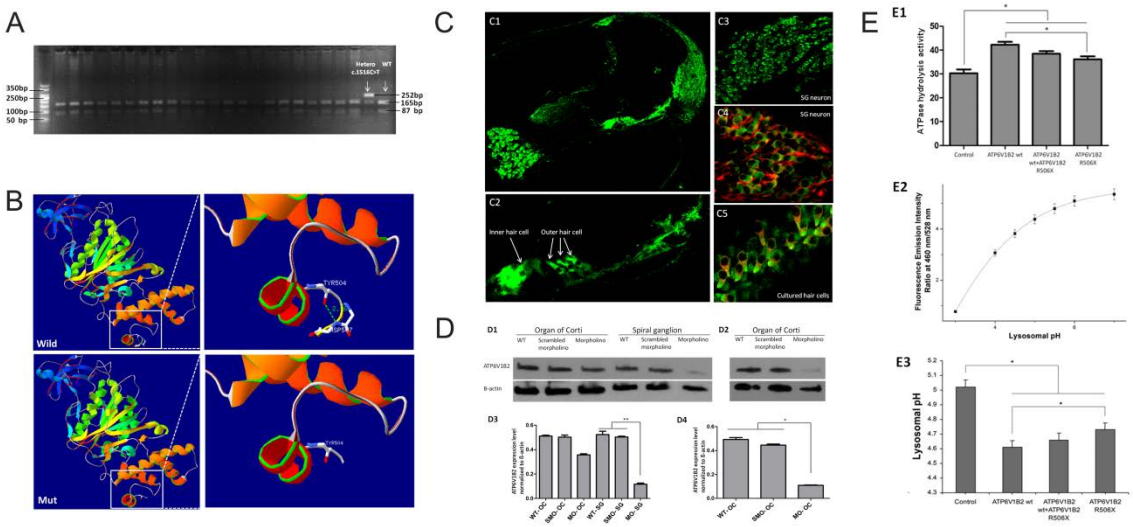

Supplementary information, Figure S1 *ATP6V1B2* c.1516 C>T mutation analysis and *Atp6v1b2* expression analysis in mouse cochlea.

Figure S1A. Taq Ⅰ restriction enzyme assay showing normal versus *ATP6V1B2* c.1516 C>T mutant PCR fragments. Example gel showing that three bands, 252bp, 165bp and 87bp, in individual with heterozygous *ATP6V1B2* c.1516 C>T mutation, and two bands, 165bp and 87bp, in wild-type controls. The pair of primers used for restriction enzyme reaction was designed around *ATP6V1B2* c.1516 C, which can amplify a fragment of 252bp. The restriction enzyme Taq I recognizes the 'TC' at c.1515 and c.1516. After the Taq I reaction, the 252bp fragment is cut into two fragments of 165 and 87 bp. However, the mutation c.1516 C>T deletes the Taq I restriction endonuclease site. Thus, for the heterozygous c.1516 C>T mutation, three bands (252, 165 and 87 bp) were detected, while in controls lacking the c.1516 C>T mutation, two bands (165 and 87 bp) were detected.

Figure S1B. Structure analysis of the wild-type ATP6V1B2 and mutant ATP6V1B2. *ATP6V1B2* p.Arg506X results in failure of hydrogen bond formation between Tyr 504 and Asp 507 in ATP6V1B2 (by Swiss model Workspace: http://swissmodel.expasy.org/workspace/).

Figure S1C. *Atp6v1b2* expression in the cochlea. (1) Atp6v1b2 distribution in adult (P30) mouse cochlea. Atp6v1b2 expresses mainly in the organ of Corti, spiral ganglion neurons, the limbus, and fibrocytes close to the stria vascularis; (2) Atp6v1b2 expression in hair cells; (3) Atp6v1b2 expression in the spiral ganglia (SG) neurons; (4) Double staining of Atp6v1b2 and tubulin in ganglia neurons. Green: Atp6v1b2, Red: ß-tubulin; (5) Double staining of Atp6v1b2 and Myo6 in cultured hair cells. Green: Atp6v1b2, Red: Myo6

Figure S1D. Protein levels of ATP6V1B2 in two regions of the cochlea from wild-type, scrambled-morpholino-control and *Atp6v1b2*-knockdown mice. (1) Western blots of ATP6V1B2 in the organ of Corti (OC) and spiral ganglion (SG) of wild-type (WT), scrambled-morpholino-oligomer (SMO, 0.5 µg/µl) control and *Atp6v1b2*-specific morpholino oligomer (MO, 0.5 µg/µl)-knockdown mice. Legends for each lane are shown in the figure. Protein was extracted from the postnatal day 9 (P9) mouse cochlea 7 days after inner ear injection. (2) Western blots of ATP6V1B2 in the organ of Corti (OC) of wild-type (WT), scrambled-morpholino-oligomer (SMO, 0.5 µg/µl) control and *Atp6v1b2*-specific-morpholino-oligomer (MO, 0.5 µg/µl)-knockdown mice. Legends for each lane are shown in the figure. Protein was extracted from postnatal day 23 (P23) mouse cochlea, 21 days after inner ear injection. (3) The band intensities in Fig.S1D1 were normalized to the corresponding ß-actin bands for quantification. Two asterisks on top of bars indicate significant reductions in ATP6V1B2 expression compared with the WT and SMO control in the spiral ganglion (Tukey's multiple comparison test, $P<0.01$). Data are presented as means ± standard deviation. Four biological replicates are represented in the bar graphs. (4) The band intensities in Fig.S1D2 were normalized to the corresponding ß-actin bands for quantification. The asterisk on top of the bars indicates significant reductions in ATP6V1B2 protein expression compared with the WT and SMO control in the organ of Corti (Tukey's multiple comparison test, $P<0.05$). Data are presented as means ± standard deviation. Four biological replicates are represented in the bar graphs.

Figure S1E. Effects of the ATP6V1B2 $^{p.Arg506X}$ mutant on ATPase activity in transfected HEK293 cells. (1) ATPase assays showed that ATPase hydrolysis activity decreased

significantly in the transfected cells as the ratio of the mutant increased. The data in each group represent a sample size (n) of 9. The asterisk on the top of bars indicates a significant increase or reduction in ATPase hydrolysis activity (P<0.05), compared to the empty vector control pIRES2-EGFP or pIRES2-EGFP-*ATP6V1B2,* respectively. Statistical analyses were performed by the Newman-Keuls Multiple Comparison Test. Data are presented as means ± standard deviation. (2) Calibration curve for determining the lysosomal pH in HEK 293 cells. Calibration was performed as described in the Materials and Methods to generate a curve relating to the emission intensity ratio at 460 and 528 nm using an excitation at 360 nm to lysosomal pH. Vertical bars represent standard errors of the mean of four identical samples. (3) The lysosomal pH increased in transfected cells as the ratio of the mutant increased, indicating that ATPase proton transport activity decreased as the ratio of the mutant increased. The data in each group represent a sample size (n) of 4. The asterisk on top of bars indicates significant reduction or increase in lysosomal pH (P<0.05), compared to the empty vector control pIRES2-EGFP or pIRES2-EGFP-*ATP6V1B2*, respectively. Statistical analyses were performed using the LSD Test. Data are presented as means ± standard deviation.